Conjugated Polymer/Metal Nanowire Heterostructure Plasmonic Antennas

By *Deirdre M. O'Carroll,* Carrie E. Hofmann,* and *Harry A. Atwater*

Plasmonic nanoantennas can significantly modify the direction and rate of spontaneous emission from nanoscale light emitters because of their intense, highly localized, surface plasmon resonances.[1–3] To date, various approaches have been taken to metallic nanoantenna fabrication, including lithographic printing,[4] colloidal synthesis,[5] focused ion beam milling,[2] nanoskiving,[6] and solution and template-based synthesis.[7] Controlled near-field coupling of linear plasmonic nanoantennas to nanoemitters is challenging since, typically, the nanoemitters (e.g., single molecules, nanoparticles, or quantum dots) are randomly dispersed relative to the metallic nanoantenna (via drop casting or spin-coating techniques)[2,8] or require chemical reactions that are specific to the metal–emitter material system.[5]

In this work, single plasmonic nanowire antennas are employed to modify the spontaneous emission spectrum, polarization direction, and emission lifetime of single monolithically coupled poly(3-hexylthiophene), P3HT, conjugated polymer nanoparticles (see Fig. 1, schematic). P3HT nanoparticle light emitters are coupled to the metal nanowire antennas by template-directed sequential electrodeposition, which consists of cathodic electrodeposition of gold nanowires within nanoporous alumina templates and subsequent anodic polymerization of the 3HT monomer at the tips of the template-embedded gold nanowires. The advantages of this approach are: 1) the metal nanowire antenna and conjugated polymer nanoparticle light emitter are self-aligned (forming a gold–P3HT nanowire heterostructure); 2) the emitter is directly integrated onto the end of the gold nanowire antenna, where highly localized longitudinal surface plasmon mode fields are expected to be strongest; 3) both the diameter and lengths of the emitter and the metal nanowire antenna can be controlled by varying template pore diameter and electrodeposition time (furthermore, these critical dimensions are not limited by the resolution of lithographic techniques); and 4) the templating route is applicable to a wide variety of light-emitting semiconductors and metals.[7] Comprehensive optical characterization and theoretical modeling are employed to demonstrate plasmonic nanoantenna-mediated light emission from P3HT nanoparticles. This work presents a simple route to fabricate discrete optical emitter–nanoantenna structures with controlled dimensions and composition, which are desirable for nanoscale optical signal routing and integrated photonic circuitry as well as plasmonic amplifiers and resonators.[9]

Figure 1a (bottom panel) is a scanning electron microscopy (SEM) image of a single gold–P3HT nanowire heterostructure fabricated by sequential deposition of gold and P3HT within the cylindrical pores of a nanoporous alumina template (see Experimental for further details). The P3HT segment remained

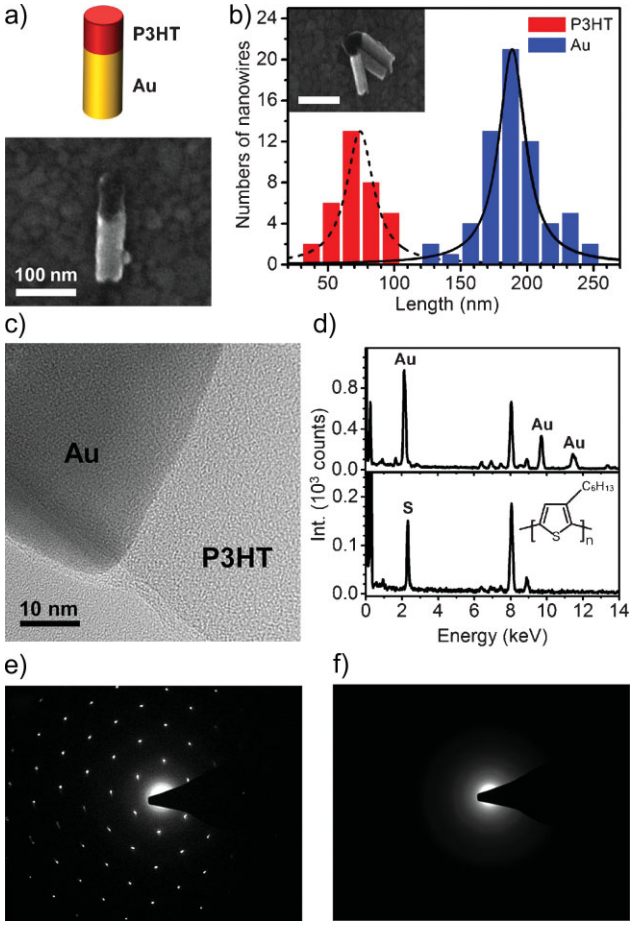

Figure 1. Top left: Schematic of a gold–P3HT nanowire heterostructure. a) SEM image of a single gold–P3HT nanowire on a gold film. b) Histograms of gold (blue) and P3HT (red) segment lengths. Inset: SEM image of gold–P3HT nanowires. Scale bar is 200 nm. c) High-resolution TEM image of a gold–P3HT interface. d) EDX spectra of gold (top) and P3HT (bottom) nanowire segments. Inset: Molecular structure of the P3HT monomer repeat unit. e) and f) SAED patterns from a gold nanowire segment (with long axis oriented in a northwest-southeast direction) and a P3HT nanowire segment, respectively.

[*] Dr. D. M. O'Carroll, C. E. Hofmann, Prof. H. A. Atwater
Thomas J. Watson Sr. Laboratory of Applied Physics, California Institute of Technology
1200 East California Blvd., MC 128-95, Pasadena, CA 91125 (USA)
E-mail: doc@caltech.edu

DOI: 10.1002/adma.200902024

in-line with the gold nanowire following template removal and nanowire dispersion. Statistical analysis of more than 50 nanowires yielded average gold and P3HT segment lengths of 190 ± 26 and 74 ± 25 nm, respectively (Fig. 1b; with average diameters of 55 ± 12 and 49 ± 12 nm, respectively).

High-resolution transmission electron microscopy (TEM) of gold–P3HT interfaces showed that the P3HT segment was in direct physical contact with the gold nanowire segment as expected, since the gold nanowire acted as a local electrode for polymerization of the 3HT monomer from solution (Fig. 1c). The interface was regular with no evidence of intermixing of the two materials or nanoparticles of gold embedded in the polymer segment. Energy dispersive X-ray (EDX) spectra acquired from gold (Fig. 1d, top panel) and P3HT (Fig. 1d, bottom panel) nanowire segments exhibited peaks from gold and sulfur, respectively, the latter originating from P3HT which contains a sulfur heterocycle in its monomer repeat unit (Fig. 1d, inset). A selected area electron diffraction (SAED) from a gold nanowire, with the long axis oriented in a northwest-southeast direction, exhibited sharp spots indicating that the region was single crystalline with preferred growth orientation along the [111] direction (Fig. 1e).[10] A SAED pattern of a P3HT nanowire region exhibited a broad diffuse halo, which suggested that the polymer material was amorphous (Fig. 1f).

Initially, optical measurements were carried out to compare the extinction and photo luminescence (PL) emission spectra of neat electropolymerized P3HT nanowires (i.e., not physically coupled to a gold nanowire) to those of P3HT thin films. Subsequently, emission spectra of gold–P3HT nanowires were compared with those of the neat P3HT nanowires. The π–π^* absorption band of a neat electropolymerized P3HT nanowire mat was slightly broader and blue-shifted in comparison to that of an as-spun P3HT thin film, with a weak shoulder at ~615 nm assigned to the more ordered, regioregular chain conformation of P3HT (Fig. 2a).[11] The tail in the absorption spectrum above 620 nm was attributed to light scattering from the nanowire mat. The PL spectrum of a single neat P3HT nanowire (see true color PL image, Fig. 2a inset) was slightly blue-shifted compared to the thin-film PL spectrum and exhibited two peaks located at 645 and 700 nm (attributed to the $S_1 \rightarrow S_0$ 0–0 and 0–1 singlet exciton transitions of regioregular P3HT, respectively),[12] and a full-width-at-half-maximum (FWHM) of 125 nm. The relative PL intensity of the 0–0 and 0–1 peaks (i.e., I_{0-0}/I_{0-1}) varied from 0.9 to 1.2 for the films and neat nanowires.

Polarization-resolved PL emission spectra from a gold–P3HT nanowire are shown in Figure 2b. The transversely polarized (I_y) PL spectrum exhibited two main peaks at about 650 and 725 nm, a FWHM of 130 nm, and an I_{0-0}/I_{0-1} value of 0.7 similar to that of the P3HT film and nanowire spectra. The longitudinally polarized (I_x) PL spectrum—main peak at 662 nm—was significantly modified in shape compared to the transversely polarized PL spectrum, exhibiting a FWHM of only 68 nm and a significantly larger I_{0-0}/I_{0-1} value of 2.6. This suggested that

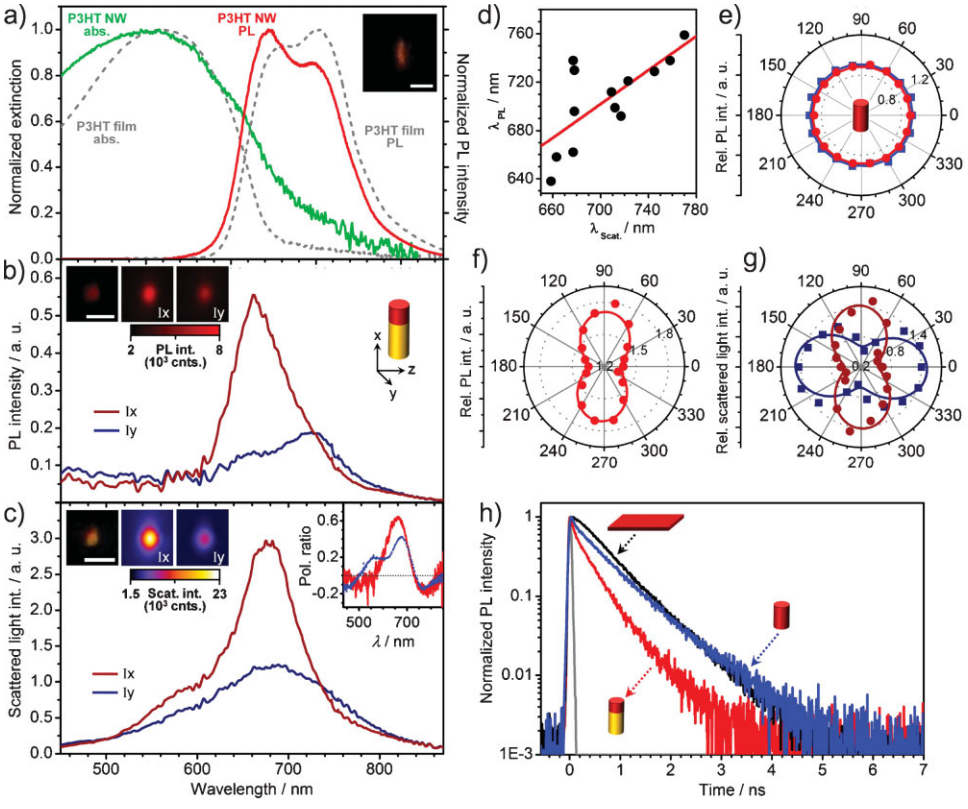

Figure 2. a) Normalized extinction and PL spectra of a P3HT thin film (dashed lines) and neat P3HT nanowires (solid lines). Inset: true color PL image of a P3HT nanowire. b,c) PL and scattered light spectra, respectively, from a single gold–P3HT nanowire with longitudinally (i.e., along *x*-axis; see right schematic inset of (b); dark red curves) and transversely (*y*-axis; dark blue curves) polarized collection. Insets at left in (b) and (c): true color total intensity (leftmost) and false color polarized intensity (rightmost) PL/scattered light images of a single gold–P3HT nanowire. Right inset of (c): Plot of PL and scattered light polarization ratios versus wavelength for a gold–P3HT nanowire (red solid and blue dashed curves, respectively; dashed line indicates zero value). d) Plot of PL wavelength versus scattered light wavelength (both at maximum intensity) for multiple gold–P3HT nanowires with linear fit. e) Polar plot of relative PL intensity at 700 nm from a single P3HT nanowire as a function of excitation (squares) and collection (circles) polarization angle. f,g) Polar plot of relative PL intensity (PL peak maximum at 700 nm for this nanowire) and relative scattered light intensity (at 540 nm (squares) and 700 nm (circles)) from a single Au–P3HT nanowire as a function of collection polarization angle, respectively. Cosine squared fits to the data points are included in all polar plots (solid lines). All relative intensity data was plotted relative to the intensity at 640 (e) or 650 nm (f,g). The nanowire long axis was vertically oriented for all polar plots as indicated by the schematic inset in (e). h) PL lifetime decays of a P3HT thin film (black), a single P3HT nanowire (blue), and a gold–P3HT nanowire (red) along with the instrument response function (IRF) of the PL lifetime system (grey). All scale bars are 1 μm.

longitudinally polarized PL from the P3HT nanoparticle was modified by the close proximity to the gold nanowire end. PL intensity images showed diffraction limited anisotropically polarized light emission from the gold–P3HT nanowire with PL intensity strongest for the longitudinal polarization (Fig. 2b, left insets). The average emission intensity enhancement of a P3HT nanoparticle coupled to a gold nanowire compared to that of a neat P3HT nanowire was estimated to be 1.8 by taking a ratio of the total PL intensity from individual gold–P3HT nanowires normalized to the P3HT emitting volume and the total PL intensity from neat P3HT nanowires normalized to their emitting volumes (using the same laser excitation power density).

To relate the features observed in the gold–P3HT nanowire emission spectra with local surface plasmon resonances of the gold nanowire, polarization-resolved scattered light spectra of the same gold–P3HT nanowire shown in Figure 2b were acquired (Fig. 2c). The transversely polarized scattered light spectrum exhibited a FWHM of about 180 nm with a main peak at 690 nm and a shoulder at ~580 nm. The longitudinally polarized spectrum exhibited a narrower peak (FWHM of 88 nm) centered at 677 nm (indicative of a longitudinal surface plasmon resonance of the gold nanowire) which overlapped substantially with the emission band of P3HT. The right inset in Figure 2c is a plot of polarization ratio, ρ (where $\rho = (I_x - I_y)/(I_x + I_y)$),[13] versus wavelength for both PL and scattered light from the same gold–P3HT nanowire. The PL polarization ratio exhibited a peak at 662 nm ($\rho = 0.63$ which represents strongly anisotropic emission polarized along the nanowire long axis) and was nearly co-incident with the dominant scattered light polarization ratio peak at 676 nm. The lower polarization ratio values of the scattered light may be due to the different excitation geometries employed for PL and scattered light measurements (see Supporting Information). For the latter, both transverse and longitudinal surface plasmon resonances are likely to be excited and contribute to the polarized scattered light signal at the detector because of the large solid angle (118°) over which the scattered light signal is both excited and collected in the far-field. This is supported by the existence of an additional peak at about 560 nm. Additionally, the P3HT emission originates from a much smaller volume localized at the end of the gold nanowire, while the scattered light signal is localized over the entire gold wire.

The PL wavelength at maximum intensity from multiple gold–P3HT nanowires (with spectral FWHM of less than 100 nm) increased almost linearly with scattered light wavelength, consistent with P3HT PL emission that was coupled to a longitudinal surface plasmon resonance of the gold nanowire, which occurs at a wavelength that varies somewhat due to the distribution of gold nanowire lengths (Fig. 2d). The greater deviation of points from a linear dependence at shorter wavelengths may be due to a contribution to the scattered light spectra from transverse or high-order multipole surface plasmon resonances.[14]

While the PL intensity from single neat P3HT nanowires varied with polarization angle and was strongest when polarized parallel to the long axis of the nanowire (Supporting Information; suggesting that some of the emitting polymer chains may be preferentially aligned parallel to the nanowire), the PL spectral shape did not change with excitation or emission polarization angle as indicated by the isotropic polarization dependence of relative PL intensity (i.e., normalized to the intensity at 640 nm) shown in Figure 2e. However, relative emission intensity from a single gold–P3HT nanowire notably varied with collection polarization angle and was preferentially polarized along the longitudinal axis (Fig. 2f). By comparison, the dependence of the relative emission intensity from the gold–P3HT nanowire on laser excitation polarization was very weak suggesting that at the laser excitation wavelength (375 nm) the P3HT absorption was not influenced by surface plasmon modes of the gold nanowire antenna (see Supporting Information).[15] The relative scattered light intensity at 540 and 700 nm from the same gold–P3HT nanowire (acquired as a function of collection polarizer angle) were almost orthogonally dependent on collection polarizer angle, as expected for transverse and longitudinal surface plasmon resonances (Fig. 2g). The longitudinally polarized PL and scattered light exhibited similar polarization dependence, which supports the assertion that the anisotropic emission from the gold–P3HT nanowire arose due to longitudinal surface plasmon-mediated emission caused by the near-field proximity of the P3HT nanoemitter to the end of the gold nanowire which functions like a sub-wavelength optical antenna (in the wavelength range of the nanoemitter).[2,3]

PL lifetime decays of neat P3HT nanowires and gold–P3HT nanowires were measured by time-correlated single photon counting and are compared in Figure 2h along with the PL lifetime of a P3HT thin film. The average PL lifetime of P3HT nanowires was 720 ± 115 ps, which was comparable to that of the P3HT thin film (600 ± 40 ps) and was consistent with literature values for the solid-state, room-temperature PL lifetime of P3HT—typically between 480 and 800 ps (depending on regioregularity, crystallinity, processing history, etc.).[12] The average PL lifetime of gold–P3HT nanowires was notably shorter at 415 ± 60 ps. This represented an increase in the total decay rate, Γ_t, ($\Gamma_t = (\Gamma_r + \Gamma_{nr})$ where Γ_r and Γ_{nr} are the radiative and nonradiative decay rates, respectively) by a factor of ≈1.7 for the P3HT nanoemitters following coupling to gold nanowires. The origin of this increase could be due to enhancement in either Γ_r or Γ_{nr} since the relative contribution of each depends on distance from the gold nanowire end due to variations in the degree to which excitons are either absorbed nonradiatively by the metal at the gold–P3HT interface or are coupled to far-field radiation farther away from the interface. Since PL intensity of P3HT nanoparticles coupled to gold nanowires is enhanced by a factor of 1.8, on average, as described earlier, it is likely that radiative decay rate is predominantly enhanced in the P3HT segment. This will be investigated further using full-field electromagnetic simulations in the latter part of the paper.

To assign the order of the longitudinal gold nanowire resonance observed in the measured scattered light spectra, theoretical *x*-polarized electric field intensity versus gold nanowire length for a 60 nm diameter cylindrical gold–P3HT nanowire was calculated (full-field, 3D, finite-difference-time-domain (3D-FDTD) simulations). Plane wave excitation (at 670 nm) incident at normal (i.e., 0°), 45°, and 80° (Fig. 3a, curves from top to bottom) was employed, since coupling to even integer multiples of half-wavelength longitudinal surface plasmon resonances (i.e., symmetric modes) strongly depends on the incident angle of excitation. Field intensity was monitored at a point within the P3HT segment 10 nm for the gold nanowire end.

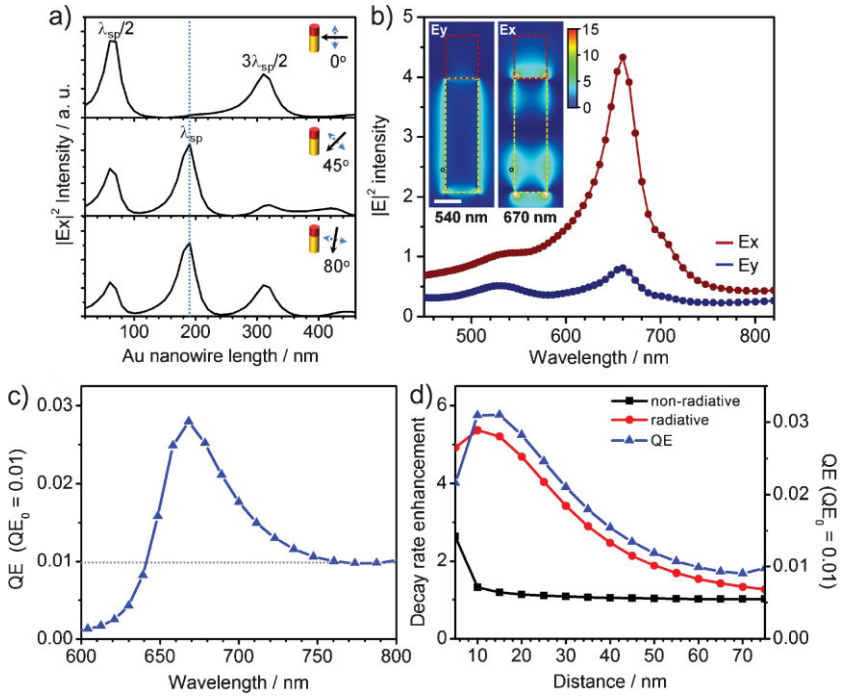

Figure 3. a) Theoretical plots of *x*-polarized near-field intensity as a function of gold nanowire length (diameter = 60 nm) under plane wave excitation at 670 nm for three different angles of incidence, 0°, 45°, and 80° with respect to the nanowire normal direction (top through bottom curves; 3D FDTD simulations). Near-field intensity was monitored at a point 10 nm from the gold nanowire end within a P3HT segment. The blue dashed line indicates a gold nanowire length of 190 nm corresponding to the synthesized nanowires. b) Theoretical near-field total intensity spectra calculated at a point 5 nm from the surface of a gold–P3HT nanowire (indicated by black circles in insets) for *y*- and *x*-polarized plane wave excitation at 45° incidence (dark blue and dark red curves, respectively). Leftmost inset: *y*-polarized field intensity cross-section at 540 nm. Rightmost inset: *x*-polarized field intensity cross-section at 670 nm. c) Theoretical *QE* for a broadband dipole emitter placed within a 75 nm long P3HT segment at a distance of 10 nm from the end of a 190 nm long gold nanowire. QE_0 of 0.01 for P3HT was assumed (dashed line). d) Nonradiative (squares) and radiative (circles) decay rate enhancements and *QE* of a dipole emitter in P3HT at 670 nm as a function of distance from the end of a gold nanowire. A background refractive index of 1.48 was employed for all 3D-FDTD simulations.

At normal incidence, the $\lambda_{sp}/2$ and $3\lambda_{sp}/2$ (where λ_{sp} is the surface plasmon wavelength) longitudinal resonant modes are excited for gold nanowires with lengths of 65 and 310 nm due to their asymmetric mode profiles.[14] At off-normal incidence, the λ_{sp} (i.e., full-wave) resonance may also be excited for gold nanowires 190 nm in length, which corresponds to the average gold nanowire length employed here. Therefore, the dominant resonance observed in the scattered light spectra of Figure 2c can be attributed to the full-wave resonance of the gold nanowire antenna.

The theoretical transverse and longitudinal near-field spectra of a 190 nm long gold nanowire exhibited two peaks at 530 and 660 nm and a weak shoulder at 700 nm (Fig. 3b; plane wave excitation incident at 45° to the nanowire long axis). For the longitudinal spectrum, the peak at 660 nm, assigned to the full-wave longitudinal resonance of the gold nanowire, was more intense by a factor of 5. For nanowires ranging from 150 to 240 nm in length, a full-wave resonance should occur in the range of 640–780 nm, which is consistent with the range of scattered light wavelength maxima observed for the gold–P3HT nanowires (see Fig. 2d). The insets in Figure 3b show E_y and E_x, near-field intensity cross-sections for *y*-polarized excitation at 540 nm and *x*-polarized excitation at 670 nm, respectively. The transverse surface plasmon mode fields (i.e., E_y fields) were strongly localized at the interface between the nanowire long axis and its environment. In contrast, the longitudinal surface plasmon mode fields (i.e., E_x fields) exhibited a standing wave profile (corresponding to the full-wave resonance of the gold wire antenna) with near-field intensity strongly localized at the nanowire ends—decaying into the P3HT segment over a distance of ~50 nm.

To further consider the relative contributions of radiative and nonradiative decay channels in the gold–P3HT nanowires, 3D-FDTD calculations of Γ_t and Γ_r of a dipole emitter within the P3HT segment were carried out (see Supporting Information) and were then used to determine the apparent quantum efficiency (*QE*) as follows:[3,17]

$$QE = \frac{\Gamma_r/\Gamma_r^0}{\Gamma_{nr}/\Gamma_r^0 + \Gamma_r/\Gamma_r^0 + ((1 - QE_0)/QE_0)}$$

where Γ_r^0 is the decay rate in the absence of the gold–P3HT nanowire and QE_0 is the intrinsic quantum efficiency of the dipole emitter. For P3HT, QE_0 is assumed to be ~0.01.[18] *QE* exhibits a value of almost 3% at 670 nm, which coincides with the full-wave resonance of the gold nanowire (Fig. 3c). The dependence of the decay rate enhancements (i.e., decay rates normalized to those of a dipole emitter in P3HT without the gold nanowire—thereby yielding information on changes in the decay rate that occur solely due to the gold nanowire antenna) and *QE* at 670 nm versus distance from the gold nanowire end is plotted in Figure 3d. It is apparent that three regimes of emission occur within the P3HT nanoemitter, which vary as a function of distance from the gold nanowire end. Below 10 nm, nonradiative decay is expected to become the dominant de-excitation pathway in the P3HT segment due to energy transfer caused by absorption in the metal, as is indicated by the enhanced Γ_{nr} and the drop off in *QE* at small distances. From 10–50 nm, the radiative decay rate enhancement dominates due to strong local field enhancement at the gold nanowire ends and, in this regime, *QE* is largest. Above 50 nm the emission from P3HT is expected to be largely unaffected by the presence of the gold nanowire, and, hence, $QE \sim QE_0$. These calculations suggest that the lifetime shortening observed in the PL lifetime data for gold–P3HT nanowires was primarily due to enhancement in the P3HT PL quantum efficiency in the region of 5–50 nm from the end of the gold nanowire antenna.

In conclusion, polythiophene nanoparticle emitters were end-coupled to single gold nanowire antennas using nanoporous template-based sequential electrodeposition. The emission

spectrum, polarization direction, and emission lifetime of the coupled polythiophene nanoparticles were substantially modified with respect to uncoupled polythiophene nanowires and thin films. The emission properties of the polythiophene nanoparticles were most strongly influenced by longitudinal surface plasmon resonances of the gold nanowire antennas due to direct placement at the ends of the antennas and overlap between longitudinal antenna resonance wavelengths and the emission band of polythiophene. Controlled placement of sub-wavelength light-emitting conjugated polymer semiconductors at the ends of plasmonic nanowires offers a useful platform for the design and realization of more complex and efficient sub-wavelength optical antennas.

Experimental

Gold–Polythiophene Nanowire Synthesis: Gold–P3HT nanowires were prepared by sequential electrodeposition of gold and polymerization of 3HT within nanoporous alumina templates (55 ± 6 nm nominal pore diameter; Synkera Technologies, Inc.). A 400 nm thick thermally evaporated layer of nickel served as a sacrificial working electrode to the pores of the alumina template. A 1 mm diameter steel wire counter electrode was placed within 3 mm of the nanoporous template surface during electrochemical deposition. Firstly, sacrificial nickel nanowires were electrodeposited in the alumina nanopores at -0.15 mA for 60 s (Keithley 286 source measure unit). Gold nanowires were then electrodeposited -0.3 mA for 15 pulses (1 s duration, 50% duty cycle, 0 mA bias). For subsequent deposition of P3HT, 3-hexylthiophene (3HT) monomer (Sigma–Aldrich) was electropolymerized at the tips of the gold nanowires at $+0.08$ mA for 5 pulses (1 s duration, 50% duty cycle, 0 mA bias) from a 20 g L^{-1} solution of in boron trifluoride diethyl etherate ($BF_3O(C_2H_5)_2$), which serves as both the solvent for 3HT as well as the supporting electrolyte [19]. The gold–P3HT nanowires were released from the template by chemically etching the nickel ($FeCl_3$ solution, 10 min), dissolving the alumina (500 mL NaOH, 3 M, 1 h), rinsing the nanowire residue with deionized water and, finally, dispersing the nanowires in isopropyl alcohol by ultrasonication (10–30 s). Neat P3HT nanowires were prepared under similar conditions, but without the gold nanowire electrodeposition step (see Supporting Information).

Optical Spectroscopy: For all PL measurements, nanowires were drop-deposited on a glass cover slip from a dispersion, allowed to dry, and then encapsulated in optical epoxy (refractive index, *n*, of 1.48; Norland Optical Adhesive 65, Norland Products, Inc.) to minimize photodegradation. Single nanowire optical measurements were taken on an inverted microscope equipped with a spectrometer consisting of a 150-mm-focal-length monochromator and liquid-nitrogen-cooled charge-coupled device (CCD) camera. For single nanowire PL lifetime measurements, a time-correlated single photon counting (TCSPC) module was employed with a 375 nm picosecond laser diode (1.5 mW, 70–300 ps pulse duration, 40 MHz) as the excitation source and a single photon avalanche diode detector as the sensing input to the TCSPC module (Picoquant GmbH). An excitation spot area of about 1.6×10^{-6} cm^2 was typically employed. The IRF exhibited a half width of ~80 ps. A $100\times$ oil immersion bright-field objective (numerical aperture of 1.3) was used for both scattered light and PL spectroscopy (see Supporting Information).

Acknowledgements

This work was supported by the US Air Force Office of Scientific Research under Grant FA9550-06-1-0480. We also acknowledge use of facilities of the Center for Science and Engineering of Materials, an NSF Materials Research Science and Engineering Center at Caltech. D.M.O'C. acknowledges support from a Marie Curie International Outgoing Fellowship within the 7th European Community Framework Programme (ACTOSPED project; PIOF-GA-2008-221230). We thank Carol Garland for TEM assistance and Keisuke Nakayama for initially supplying porous alumina templates. Supporting Information is available online from Wiley InterScience or from the author.

Received: June 17, 2009
Published online: December 15, 2009

[1] M. Ringler, A. Schwemer, M. Wunderlich, A. Nichtl, K. Kürzinger, T. A. Klar, J. Feldmann, *Phys. Rev. Lett.* **2008**, *100*, 203002.
[2] T. H. Taminiau, F. D. Stefani, F. B. Segerink, N. F. Van Hulst, *Nat. Photon.* **2008**, *2*, 234.
[3] L. Rogobete, F. Kaminski, M. Agio, V. Sandoghdar, *Opt. Lett.* **2007**, *32*, 1623.
[4] a) S. A. Maier, M. L. Brongersma, P. G. Kik, S. Meltzer, A. A. G. Requicha, H. A. Atwater, *Adv. Mater.* **2001**, *13*, 1501. b) K. B. Crozier, A. Sundaramurthy, G. S. Kino, C. F. Quate, *J. Appl. Phys.* **2003**, *94*, 4632.
[5] T. Mokari, E. Rothenberg, I. Popov, R. Costi, U. Banin, *Science* **2004**, *304*, 1787.
[6] X. Qiaobing, J. Bao, F. Capasso, G. M. Whitesides, *Angew. Chem.* **2006**, *118*, 3713.
[7] a) J. J. Mock, S. J. Oldenburg, D. R. Smith, D. A. Schultz, S. Schultz, *Nano Lett.* **2002**, *2*, 465. b) J. C. Hulteen, C. R. Martin, *J. Mater. Chem.* **1997**, *7*, 1075. c) S. R. Nicewarner-Pena, R. G. Freeman, B. D. Reiss, L. He, D. J. Pena, I. D. Walton, R. Cromer, C. D. Keating, M. J. Natan, *Science* **2001**, *294*, 137. d) O. Reynes, S. Demoustier-Champagne, *J. Electrochem. Soc.* **2005**, *152*, D130.
[8] V. Akimov, A. Mukherjee, C. L. Yu, D. E. Chang, A. S. Zibrov, P. R. Hemmer, H. Park, M. D. Lukin, *Nature* **2007**, *450*, 402.
[9] a) S. A. Maier, P. G. Kik, H. A. Atwater, S. Meltzer, E. Harel, B. E. Koel, A. A. G. Requicha, *Nat. Mater.* **2003**, *2*, 229. b) M. I. Stockman, *Nat. Photon.* **2008**, *2*, 327.
[10] M. Tian, J. Wang, J. Kurtz, T. E. Mallouk, M. H. W. Chan, *Nano Lett.* **2003**, *3*, 919.
[11] a) T. A. Chen, X. Wu, R. D. Rieke, *J. Am. Chem. Soc.* **1995**, *117*, 233. b) P. J. Brown, D. S. Thomas, A. Köhler, J. S. Wilson, J.-S. Kim, C. M. Ramsdale, H. Sirringhaus, R. H. Friend, *Phys. Rev. B* **2003**, *67*, 064203. c) M. Leclerc, F. M. Diaz, G. Wegner, *Makromol. Chem.* **1989**, *190*, 3105. d) E. L. Ratcliff, J. L. Jenkins, K. Nebesny, N. R. Armstrong, *Chem. Mater.* **2008**, *20*, 5796.
[12] a) G. Rumbles, I. D. W. Samuel, L. Magnani, K. A. Murray, A. J. DeMello, B. Crystall, S. C. Moratti, B. M. Stone, A. B. Holmes, R. H. Friend, *Synth. Met.* **1996**, *76*, 47. b) N. P. Wells, B. W. Boudouris, M. A. Hillmyer, D. A. Blank, *J. Phys. Chem. C* **2007**, *111*, 15404. c) K. Kanemoto, T. Sudo, I. Akai, H. Hashimoto, T. Karasawa, Y. Aso, T. Otsubo, *Phys. Rev. B* **2006**, *73*, 235203.
[13] J. R. Lakowicz, *Principles of Fluorescence Spectroscopy*, 2nd ed., Kluwer Academic/Plenum, New York, NY **1999**.
[14] a) E. R. Encina, E. A. Coronado, *J. Phys. Chem. C* **2007**, *111*, 16796. b) L. Novotny, *Phys. Rev. Lett.* **2007**, *98*, 266802.
[15] H. Mertens, J. S. Biteen, H. A. Atwater, A. Polman, *Nano Lett.* **2006**, *6*, 2622.
[16] G. Schider, J. R. Krenn, A. Hoohenau, H. Ditbacher, A. Leitner, F. R. Aussenegg, W. L. Schaich, I. Puscasu, B. Monacelli, G. Boreman, *Phys. Rev. B* **2003**, *68*, 155427.
[17] a) A. Mohammadi, V. Sandoghdar, M. Agio, *New J. Phys.* **2008**, *10*, 105015. b) P. Bharadwaj, L. Novotny, *Opt. Express* **2007**, *15*, 14266.
[18] a) N. C. Greenham, I. D. W. Samuel, G. R. Hayes, R. T. Phillips, Y. A. R. R. Kessener, S. C. Moratti, A. B. Holmes, R. H. Friend, *Chem. Phys. Lett.* **1995**, *241*, 89. b) J. Piris, T. E. Dykstra, A. A. Bakulin, P. H. M. van Loosdrecht, W. Knulst, M. T. Trinh, J. M. Schins, L. D. A. Siebbeles, *J. Phys. Chem. C* **2009**, *113*, 14500.
[19] a) G. Shi, S. Jin, G. Xue, C. Li, *Science* **1995**, *267*, 994. b) G. Shi, C. Li, Y. Liang, *Adv. Mater.* **1999**, *11*, 1145. c) S. Zhang, G. Nie, X. Han, J. Xu, M. Li, T. Cai, *Electrochim. Acta* **2006**, *51*, 5738.